Numerical Simulation of a Two-Phase Cyclone Separator.

Bjørnar Rødland
Birger Haugen
Sondre Norheim

Bachelor's thesis in mechanical engineering
Bergen, Norway 2019

Høgskulen
på Vestlandet

Numerical Simulation of a Two-Phase Cyclone Separator

Bjørnar Rødland
Birger Haugen
Sondre Norheim

Department of Mechanical- and Marine Engineering
Western Norway University of Applied Sciences
NO-5063 Bergen, Norway

Numerical Simulation of a Two-Phase Cyclone Separator.
Numerisk Simulering av Tofase Syklon Separator.

Authors, student number:	Bjørnar Rødland, h181321
	Birger Haugen, h150150
	Sondre Norheim, h181342

Preface

This thesis is written as part of a bachelor's program in mechanical engineering at the department of Mechanical and Marine Engineering at Western Norway of Applied Science, campus Bergen. The thesis was in cooperation with the department and was carried out during the winter and spring of 2019. The group would like to give recognition to the following persons for contributions to the thesis:

We wish to express our sincere gratitude to our supervisor Dr. Shokri Amzin. Without his guidance and persistent support during all stages of the work the thesis would not have been possible. We also appreciate his dedication and enthusiasm towards our thesis and work.

We would like to acknowledge the contributions of Dr. Hassan Momeni for his support during this thesis, as well as his assistance during our three years at HVL.

We would also like to thank Dr. Boris Balakin for giving us the opportunity to work with the CFD software STAR CCM+, and helping us troubleshoot some of the problems we encountered and also to Dr. Gloria Stenfelt for her help with the software.

Our thanks are extended to all members at the faculty and the department for contributing to our education.

Bergen, May 2019

Bjørnar Rødland, Birger Haugen and Sondre Norheim

Høgskulen
på Vestlandet

Publications

B. Haugen, B. Rødland, S. Norheim, H. Momeni and S. Amzin, Numerical Modelling of Two-phase Flow in a Gas Separator Using Eulerian-Lagrangian Flow Model, *International Journal of Chemical Engineering*, 2019 – (Submitted, under review).

Abstract

Gravity-driven separators are broadly used in various engineering applications to remove particulate matters from gaseous fluids to meet legislation demands. This study represents a detailed numerical investigation of a two-phase cyclone separator using Eulerian-Lagrangian gas flow method. Considering the intricate vortex created by the separator, the turbulence is modelled using Reynolds Stress Modell (RSM). The simulations were conducted using the Reynolds Averaged Navier-Stokes (RANS) approach to solve the governing equations. This approach was selected because of the complexity of the separator and make it less computational demanding. For engineering purposes, this method is one of the more common approaches. The method has successfully predicted the typical trends and variations seen in such gas separators. Some factors that influence the separators efficiency were identified. This indicates that both the inlet velocity and the particle diameter greatly affect the efficiency of the separator. Also, the computed results show a realistic agreement with the experimental measurements.

Sammendrag

Gravitasjonssseparatorer brukes i ulike tekniske applikasjoner for fjerning av partikler fra forurensede gasser for å oppfylle forskjellige lovkrav. Denne studien representerer en detaljert numerisk undersøkelse av en tofase syklonseparator ved bruk av Eulerian-Lagrangian gass strømmnings modell. I separator kammeret vil en komplisert virvel oppstå, og for å modellere dens turbulens er Reynolds Stress Model (RSM) benyttet i simuleringen. Simuleringene ble utført ved hjelp av metoden Reynolds Averaged Navier-Stokes (RANS) for å løse de mest sentrale ligningene. Denne tilnærmingen ble valgt på grunn av kompleksiteten til separatoren og for å gjøre beregningene mindre maskin krevende. For typiske ingeniør prosjekt er denne metoden mest vanlig. Metoden har korrekt fått frem de typiske trendene og variasjonene som ses i slike gasseparatorer. Faktorer som påvirker separatorens effektivitet er også blitt identifisert. Disse viser at både innløpshastigheten og partikkeldiameteren sterkt påvirker separatorenes effektivitet. De beregnede resultatene samsvarer også med de eksperimentelle målingene.

Table of contents

Nomenclature

$\boldsymbol{\tau_{ij}}$	=	Viscous Stress Tensor
$\boldsymbol{\rho\overline{u_i' u_j'}}$	=	Reynolds Stress Term
$\boldsymbol{\overline{\rho}}$	=	density
$\boldsymbol{\phi_{ij}}$	=	Pressure Strain
$\boldsymbol{\epsilon_{ij}}$	=	Dissipation
$\boldsymbol{\delta_{ik}}$	=	Kroenke delta
$\boldsymbol{\mu}$	=	Molecular Viscosity of the Fluid / dynamic viscosity
$\boldsymbol{\beta}$	=	Coefficient of Thermal Expansion
$\boldsymbol{\theta}$	=	Eddy Diffusivity model
$\boldsymbol{\tau_r}$	=	Particle Relaxation Time
$\boldsymbol{\rho_p}$	=	Density of Particles
$\boldsymbol{\rho_g}$	=	Density of Air
$\boldsymbol{e}$	=	Eulers Number
$\boldsymbol{C_d}$	=	Coefficient of Drag
$\boldsymbol{d}$	=	Particle Size
$\boldsymbol{\overline{d}}$	=	Characteristic Diameter
$\boldsymbol{d_p}$	=	Diameter of Particle
$\boldsymbol{D_{T,ij}}$	=	Turbulent Diffusion
$\boldsymbol{D_{L,ij}}$	=	Molecular Diffusion
$\boldsymbol{F}$	=	Body force
$\boldsymbol{\overline{F}_i}$	=	Coupling term
$\boldsymbol{F_d}$	=	Force of Drag
$\boldsymbol{g}$	=	Gravity
$\boldsymbol{g_i}$	=	Gravity component in direction i
$\boldsymbol{G_{ij}}$	=	Buoyancy Production
$\boldsymbol{n}$	=	Distribution Parameter
$\boldsymbol{p'}$	=	Characteristic velocity
$\boldsymbol{P}$	=	Pressure
$\boldsymbol{P_{ij}}$	=	Stress Production
$\boldsymbol{Re}$	=	Reynolds Number
$\boldsymbol{t}$	=	time
$\boldsymbol{u_g}$	=	Gas Phase Velocity
$\boldsymbol{u_p}$	=	Particle Velocity
$\boldsymbol{u}$	=	velocity
$\boldsymbol{u_i}$	=	Velocity component in direction i
$\boldsymbol{\tilde{u}}$	=	Average velocity
$\boldsymbol{x}$	=	space
$\boldsymbol{x_i}$	=	Space component in direction i

1. Introduction

Air pollution is one of the ancient environmental dilemmas known to humans, as its sources vary from natural to unnatural. However, with the emergence of the Industrial Revolution in the 18th and 19th centuries, the phenomenon has since then continued to deteriorate, and air pollution has become one of the most problematic environmental challenges. The health effects of air contamination are severe, for instance, air pollution due to particulate matter (PM), nitrogen dioxide and ozone is a significant cause of severe health problems [1, 2]. Environmental legislation has thus become more stringent to improve air quality and are forcing engineers to develop an efficient industrial system.

Gravity-driven separators are extensively used in many industrial processes for their simple construction, low operation and maintenance cost and their wide range of operational conditions [3, 4]. They are typically used to remove particulate matters from gaseous fluids using centrifugal forces [5-7]. The cyclone is often part of a complete air purification unit, where the large-sized particulates are removed from the gas stream in the cyclone before being directed through further filtration devices to remove the fine particulates. Traditionally, separators are classified based on their geometry as vertical, horizontal and spherical where each has its advantages and disadvantages [8]. However, several factors must be considered when selecting an industrial separator for a given application. For instance, among those the traits of the fluid to be processed, size, transportation and the cost.

In a horizontal separator the chamber is constructed horizontally and the fluid flows in the same direction. The common components in the liquid is gas, oil and water, but not exclusively. By giving the fluid an extended retention time in the chamber, it will settle and segregate into different layers because of gravity. The gas will settle at the top of the chamber and exit by a gate valve also at the top of the separator. The water is separated from the oil by a baffle and then extracted using two dump valves placed at the bottom of the chamber.

A spherical separator is small, compact and inexpensive, but with limitations to its surge space. The fluid is introduced to a spinning chamber and the particles separates from the water and/or the gas/oil. The process is very similar to the vertical separator, but instead of the fluid spinning the chamber itself is.

Vertical separators are often chosen when the gas -liquid ratios is high, while horizontal separators are chosen when there is a large volume of total fluid with large amounts of dissolved gas in the liquid. They are also chosen for three-phase separation. A key difference between the two is how much space they occupy. Horizontal chambers are often large and take up much space unless stacked, while the vertical takes up less space, but are often tall. The spherical separator is used for high pressure cases and with small liquid volumes. A benefit is also its compact size compared to the vertical and horizontal separator [9].

In vertical separators, the untreated gas enters tangentially from the inlet at high velocity and due to the centripetal forces; the untreated stream flows circularly downwards carrying the particles. Due to the gradual reduction in the separator's cone, the gas velocity increases creating an additional inner central vortex at the centre of the separator — the inner vortex flows upward carrying the clean gas [10]. Eventually, the separated particles exit at the bottom of the separator because of their high density [5].

Advanced modelling techniques are widely used in many engineering applications to design or/and optimise practical systems [11]. They are efficient, cost-effective and can produce detailed information that is sometimes challenging and costly to produce by experiments. Computational fluid dynamics (CFD) software are also widely used and brings a lot of the same benefits as modelling techniques. The CFD analysis is used on a variety of engineering fields to solve a significant number of complex processes, such as multiphase flows. Hence, the primary objective of this study is to carry out a detailed numerical analysis using the Eulerian-Lagrangian gas flow model applied to vertical separator, and compare the results with experimental measurements [12, 13].

2. Method

2.1 Eularian-Langrangian gas flow model

In this section, the Eulerian-Lagrangian method, which is used to observe and analyse the fluid flow inside the separator, is discussed briefly.

Fluid flows can be analysed mathematically, either using the Lagrangian description where the trajectories of the individual fluid particles are tracked in time or/and using the Eulerian representation where the evolution of the fluid properties are observed at every point in space as time varies [13, 14]. To be noted, it can be computationally expensive to track all the fluid particles in a flow; therefore, only selected particle trajectories are to be tracked.

In multiphase fluids, both discerptions are combined where the gas-phase is solved in conjunction with tracking individual particles. The particles are tracked by indirectly solving transport equations using the Lagrangian particle method. The conservation of mass and momentum are represented by Eulerian conservation equations [15].

2.1.1 Gas phase flow

The equations of mass and momentum conservation are solved for the continuous phase, which in this case is the gas phase.

$$\frac{\partial \overline{\rho}}{\partial t} + \frac{\partial \overline{\rho}\widetilde{u_\iota}}{\partial x_i} = 0.$$

(1)

The first term indicates the time variation, and the second term indicates the changes due to fluid transport. ρ is the density of gas and u is the average velocity of the gas.

$$\frac{\partial(\overline{\rho}\widetilde{u_\iota})}{\partial t} + \frac{\partial(\overline{\rho}\widetilde{u_\iota}\widetilde{u_j})}{\partial x_i} = \frac{\partial \overline{P}}{\partial x_j} + \frac{\partial}{\partial x_i}\left(\tau_{ij} - \rho\overline{u_i'u_j'}\right) + \overline{F_\iota}.$$

(2)

The first term on the left-hand side (LHS) indicates the unsteady term, while the second term indicates the rate of change. On the right-hand side (RHS), the first term indicates the pressure gradient, where P is the pressure. The second term indicates the momentum due to viscous forces, where τ_{ij} is the viscous stress tensor, and $\rho\overline{u_i'u_j'}$ is the Reynolds stress term. The third term is the coupling term between the phases, and it approximates the sum of the drag on each particle occurring inside of a fluid control volume.

The dominating swirl inside the separator creates an anisotropic turbulence field. When modelling the turbulence field, the Reynolds Stress Model (RSM) is adopted [16]. The RSM provides differential transport equations for each of the Reynolds stress components.

$$\frac{\partial\left(\rho\overline{u_i'u_j'}\right)}{\partial t} + \frac{\partial\left(\rho\tilde{u}\overline{u_i'u_j'}\right)}{\partial x_k} = D_{T,ij} + D_{L,ij} + P_{ij} + G_{ij} + \phi_{ij} + \epsilon_{ij.} \tag{3}$$

$D_{T,ij}$ represents turbulent diffusion, $D_{L,ij}$ is the molecular diffusion, P_{ij} is the stress production, G_{ij} is the buoyancy production, φ_{ij} is the pressure strain, and ε_{ij} is the dissipation. These terms are a function of the mean gas phase velocity gradients.

$$D_{T,ij} = -\frac{\partial}{\partial x_k}\left[\rho\overline{u_i'u_j'u_k'} + \overline{\rho'\left(\delta_{kj}u_i' + \delta_{ik}u_j'\right)}\right]. \tag{4}$$

$$D_{L,ij} = \frac{\partial}{\partial x_k}\left[\mu\frac{\partial}{\partial x_k}\overline{\left(u_i'u_j'\right)}\right]. \tag{5}$$

$$P_{ij} = -\rho\left(\overline{u_i'u_k'}\frac{\partial u_j}{\partial x_k} + \overline{u_j'u_k'}\frac{\partial u_i}{\partial x_k}\right). \tag{6}$$

$$G_{ij} = -\rho\beta\left(g_i\overline{u_j'\theta} + g_j\overline{u_i'\theta}\right). \tag{7}$$

$$\phi_{ij} = \overline{p'\left(\frac{\partial u_i'}{\partial x_j} + \frac{\partial u_j'}{\partial x_i}\right)}. \tag{8}$$

$$\epsilon_{ij} = -2\mu\overline{\frac{\partial u_i'}{\partial x_k}\frac{\partial u_j'}{\partial x_k}}. \tag{9}$$

2.1.2 Lagrangian particle tracking

The Lagrangian method is based on a local force balance on each particle. The force balance considers the particle inertia with the forces acting on it and can be expressed as

$$\frac{du_p}{dt} = \frac{u_g - u_p}{\tau_r} + \frac{g(\rho_p - \rho_g)}{\rho_p} + F. \tag{10}$$

The LHS represents the inertial force per unit mass, where u_p is the particle velocity. On the RHS, the first term expresses the drag between the phases, where u_g is the gas phase velocity. The second term represents the gravity and buoyancy, respectively. g is the

gravity constant, and ρ_p and ρg is the density of the particle and air, respectively. The last term represents any additional forces that may act upon the particles. τ_r represents the particle relaxation time and is expressed as

$$\tau_r = \frac{\rho_p d_p^2}{18\mu} * F_d,$$ (11)

and

$$F_d = \frac{24}{C_d * Re},$$ (12)

where d_p is the particle diameter, μ is the molecular viscosity of the fluid, F_d is the drag force, C_d is the drag coefficient, and Re is the relative Reynolds number, which is defined as

$$Re \equiv \frac{\rho_g d_p |u_p - u_g|}{\mu}.$$ (13)

One-way coupling is used in the simulations, which means that the fluid phase influences the particles via aerodynamic drag. For the drag coefficient, C_d, the Schiller-Naumann model is used [17].

$$C_d = \begin{cases} \dfrac{24(1 + 0,15Re^{0,687})}{Re} & Re \leq 1000 \\ 0,44 & Re > 1000 \end{cases}.$$ (14)

2.2 Computational fluid dynamics

When using computational fluid dynamics, there are different approaches to how the governing equations are solved in the software. The available methods are Direct Numerical Simulation (DNS), Large Eddy Simulation (LES), and Reynolds Averaged Navier-Stokes (RANS). In this section, these approaches are described shortly and the pros and cons for each approach is mentioned to justify the chosen method for this study.

2.2.1 DNS – Direct Numerical Simulation

DNS is the most straightforward and obvious approach when modelling turbulent flows. When using the DNS the Navier-Stokes equations is solved directly, and they describe the fluid flows, both for laminar and turbulent conditions correctly [18]. All the equations are

20

integrally solved, without the use of any turbulence models. The method gives very detailed resolutions but demands very fine computational grids and a small timescale to be solved. This makes the DNS-method very time-consuming, and extremely computer-power demanding. With high Reynolds-numbers, this becomes even more evident, thus making this an undesirable option for practical engineering.

2.2.2 LES – Large Eddy Simulation

With high Reynolds-numbers, the presence of small length- and timescales makes the solving very demanding. By filtering the eddies and solving only for the intermediate to large eddies, it becomes less time- and power demanding. This intentionally leaves the small eddies unresolved, and models are used instead of DNS to compute these [19, 20]. Because the small eddies are most difficult to compute, the LES approach is less computational demanding than the DNS method, but the results might be less accurate.

2.2.3 RANS – Reynolds Averaged Navier-Stokes

The Reynolds Averaged Navier-Stokes or RANS method is the most used approach for numerical simulations in CFD. This is because both the LES and DNS is too computational demanding to be used for engineering purposes. The results provided by the RANS method gives an adequate accuracy and is less demanding than the others mentioned [21]. Therefore, the RANS approach is most commonly used for engineering problems and is used in this study.

Osborne Reynolds proposed that each quantity in the instantaneous Navier-Stokes equation could be separated into two parts; one mean part and one fluctuating part. This led to the Reynolds-averaging of the governing equations, and the RANS method was introduced [22]. Applying this method to non-linear equations will result in a set of new unknown terms. These new terms can be modelled with the use of different closure techniques.

2.3 Experimental setup

The computational results obtained by the CFD analysis are compared to the experimental results of Wang [12]. The experiment is conducted using air contaminated with cement particles. The contaminated air is blown into a vertical separator at a velocity of 20 m/s. A flowmeter is used to measure the flow rate. The outlets are open to the air at a pressure of 1 atm. The particle phase volume fraction is less than 10%. The density of the particles is 3320 kg/m^3. A probe is used to measure the velocity and pressure of the gas field. It is placed in the flow field with five pressure transducers to obtain voltage signals. The particle distribution of the cement material can be expressed by the Rosin-Rammler equation [23].

$$R(d) = e^{-\frac{d^n}{\bar{d}}},$$
(15)

where $R(d)$ is the mass fraction of particles with a diameter greater than d. $\bar{d}$ equals to the characteristic diameter, in this case set to 29.90 μm. n is the distribution parameter and is specified to be 0.806.

A schematic of the cyclone, along with the selected axial locations, are shown in Fig. 1. Each axial location spans 175 mm in length. The computational parameters used in this study are presented in Table. 1 The boundary conditions for the inlet is set to be as velocity inlet, while both the outlets are set to be pressure outlets.

Density of air	*1.205 kg/m³*
Density of particles	*3320 kg/m³*
The volume fraction of the discrete phase	*3%*
Pressure	*1 bar* (atmospheric)
Temperature	*300K*
Inlet velocity	*5-35 m/s*
Particle diameter	*1-5 μm*
Rosin-Rammler diameter range	*1-100 μm*

Table 1. Boundary conditions.
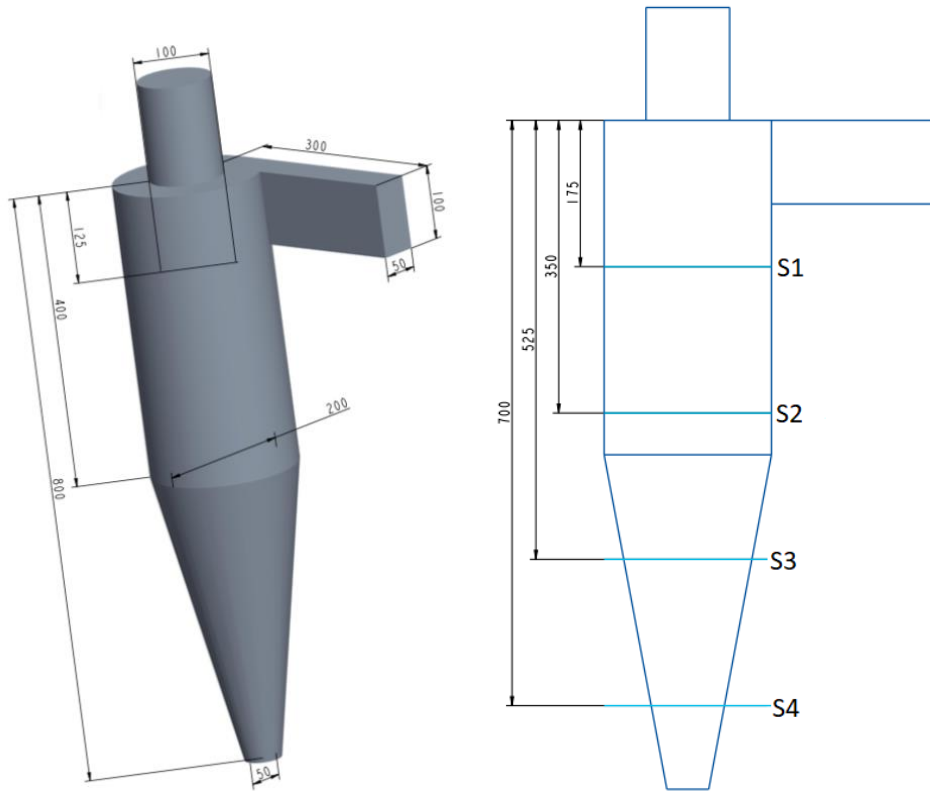
Figure 1. Schematic and the axial sections of the test cyclone [7].

2.4 Numerical setup

The computational tool used in this study is the commercial software STAR CCM+. The tool solves the steady Favre averaged transport equations Eqs. (1), (2), (3) and (10) along with their selected closures on the physical grid. The non-linear differential steady governing equations for the complex flow fields are discretised using a mixed finite element method, which employs stabilisation techniques to address issues with the pressure-velocity coupling and the non-linear convection terms.

The RSM model is used because of the intense swirl inside the separator. Since the volume fraction of the particles is low, a point-particle injector is used to add particles. For a more detailed description of the numerical setup, see Appendix 1.

2.4.1 Grid generation

In order to solve the governing equations of the fluid flow, the flow domain must usually be split up in smaller subdomains. The governing equations are then solved for each subdomain or cell. The collection of these cells is called mesh or grid.

The flow domain of the cyclone separator was meshed using prism layer mesher, surface remesher, and polyhedral mesher. Prism layer is created next to wall boundaries to improve the accuracy of the flow. Prism layer also provides good resolution of the turbulent boundary layer. The surface remesher improves the overall quality of the surface mesh and optimize it for the volume mesh by re-triangulating the existing surface.

23

The polyhedral mesher was used to mesh the entire volume of the cyclone separator, as shown in Fig. 2. Compared to tetrahedral mesh, polyhedral mesh contains approximately four times fewer cells for a given surface. Polyhedral mesh will thus have a lower computational cost [24]. Also, the sensitivity of the computed solution to the cell size and type was tested by using two different types of cells, hexahedrons and polyhedrons. It has been observed that the polyhedron cells produce a more realistic solution, as shown in Table 2. Hence, the solution presented in section 3 shows negligible grid sensitivity.

Cell type	Cells	Pressure (Pa)
Poly	39266	1417
Poly	99436	1433,1
Poly	192887	1538,7
Cubes	187558	1005,9

Table 2. Grid sensitivity test.

(a)   (b)
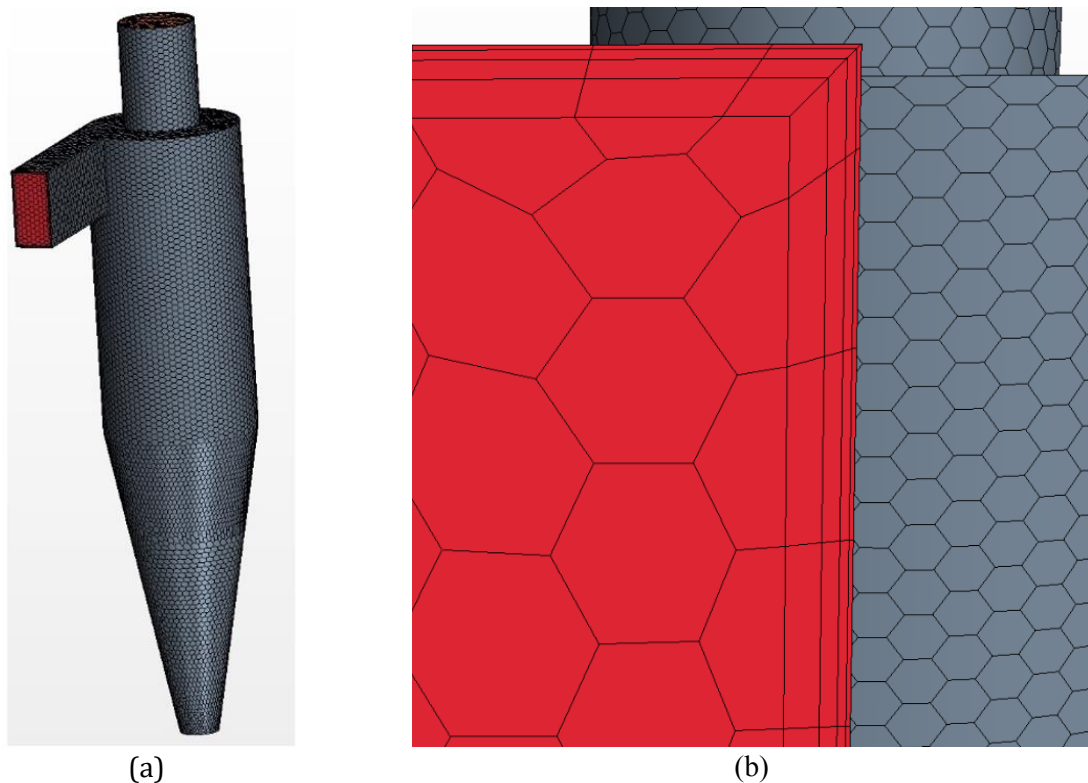
Figure 2. General generated computational grid (a) and prism layer close up (b).

2.4.2 Residuals and iterations

Two major aspects are considered to achieve convergence. Residual monitor plots are useful for judging the convergence of the solution, shown in Fig. 3. Residuals are the difference in the value of a quantity between to iterations. It is important to understand both the significance of residuals and their limitations. While it is true that the residual quantity tends to trend towards a small number when the solution is converged, the residual monitors cannot be relied on as the only measure of convergence. Residuals do not necessarily relate to variables of interest in the simulation such as velocities, pressure drop, or mass flow rates. The change in pressure drop can be monitored for every

iteration. After about 6000 iterations the monitored pressure drop is recognized to have slim fluctuations, as depicted in Fig. 4. With low changes in residuals and pressure drop being constant, the conclusion is that the simulation has converged. Convergence has been achieved for all the simulations of the cyclone separator.

Simulations are normally complete when convergence is achived at both the residual monitor and key-variable monitors, in this case about 6000 iterations. The values of engineering interest are then constant, but the particle tracking would stop when the simulation stops. To check the efficiency of the separator the simulations were set to run for two seconds. With the timestep of 0.01 the simulations need 20 000 iterations to reach 2 seconds. The simulation will run beyond its convergence point. This will have a small impact on the other results and is neglected. In a perfect simulation, it would be desirable to run it at least 10 seconds to get a more accurate value of the efficiency, but this would increase the computational demand, therefore 2 seconds is sufficient for this study.
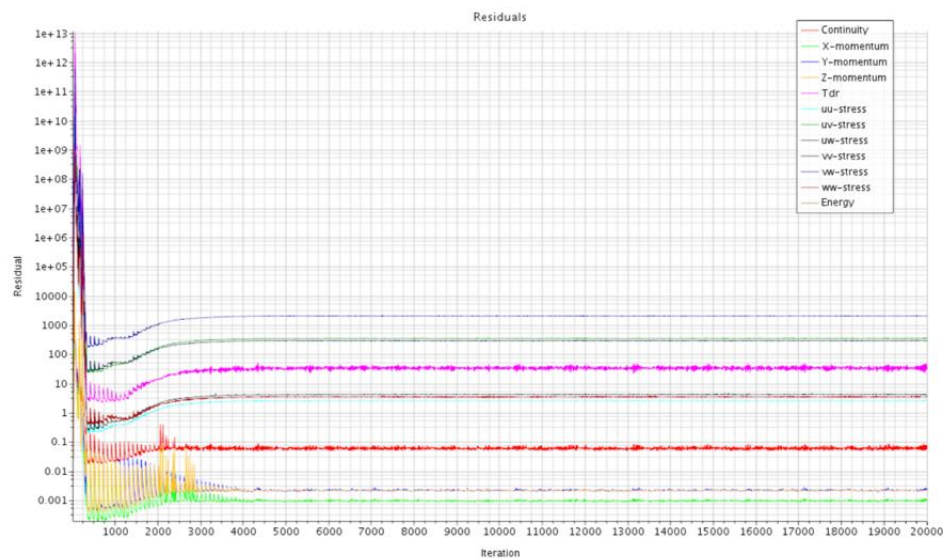
Figure 3. Residual function plot.
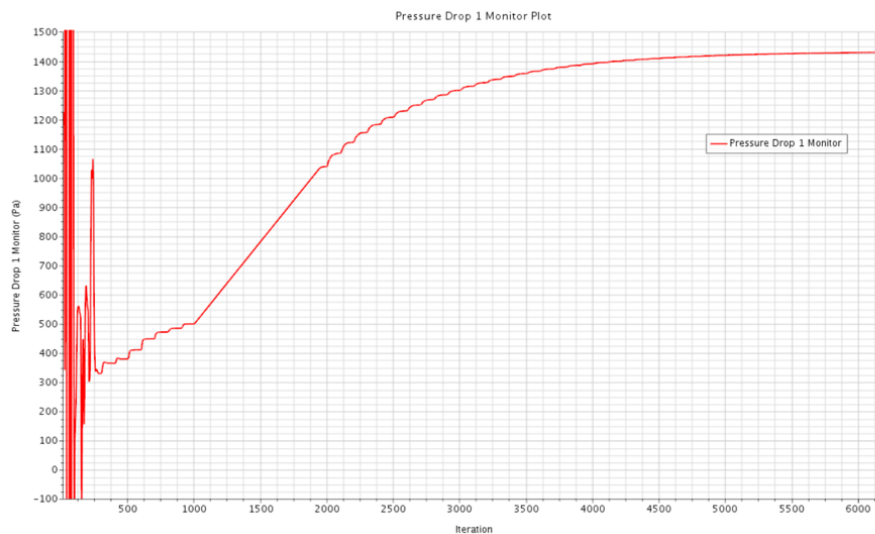
Figure 4. Pressure drop monitor point.

3. Results and discussion

3.1 Pressure drops

The pressure drop is a vital parameter in industrial separators. It can predict the total cost of operation, as a higher pressure drop will require greater power to move the fluid across the separator [25]. Fig. 5 shows the computed correlation between velocity and pressure drop inside the separator. Typically, the pressure drop increases with increasing inlet velocity. Although it is observed that the computed results are slightly lower than the measured results for low inlet velocities, the correlation improves gradually when the inlet velocity exceeds 20 *m/s*. At inlet velocity higher than 30 *m/s*, the experimental measurements are slightly over-predicted. Nevertheless, the computed pressure drop results are in good agreement with experimental measurements for all inlet velocities [12].
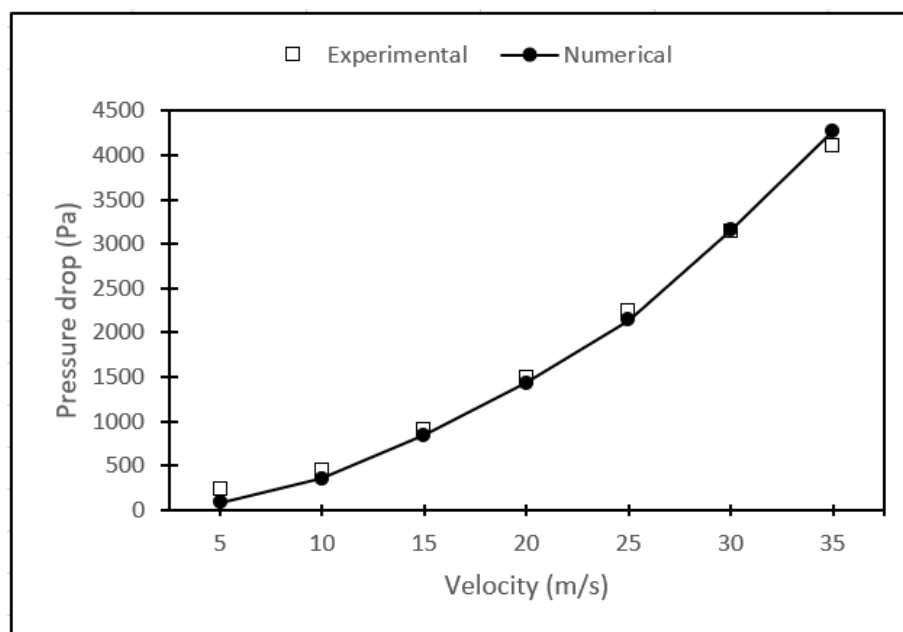
Figure 5. The computed pressure drops compared to the experimental measurements at different inlet velocities.

3.2 Tangential velocity

From the design and efficiency point of view, the tangential velocity is critical; it aids to determine the centrifugal forces inside the separator. Accordingly, the tangential velocity is computed and compared to the experimental measurements at different axial locations inside the separator. As observed in Fig. 6, the tangential velocity has an M-shaped profile at axial locations S1, S2 and S3, while V-shaped at axial location S4. A schematic of these sections can be found in Fig. 1. The tangential velocity profiles are symmetric with the axis of the separator. It is also noted that the flow creates two symmetric vortex regions known as the internal forced vortex and the external free vortex, the "Rankine Vortex" [26]. Typically, for the internal vortex, the tangential velocity increases with increasing radius, whereas it decreases with an increasing radius for the external vortex. The

computed maximum tangential velocity is approximately 1.6 the magnitude of the inlet velocity in all axial locations, which is consistent with measurements obtained by Wang [12].

The contours of the tangential velocity are shown in Fig. 7. The flow characteristics inside the separator are identical for inlet velocity less than 25 *m/s*. However, when the vortex shape changes at higher inlet velocities, the flow characteristics changes and the flow become asymmetric.
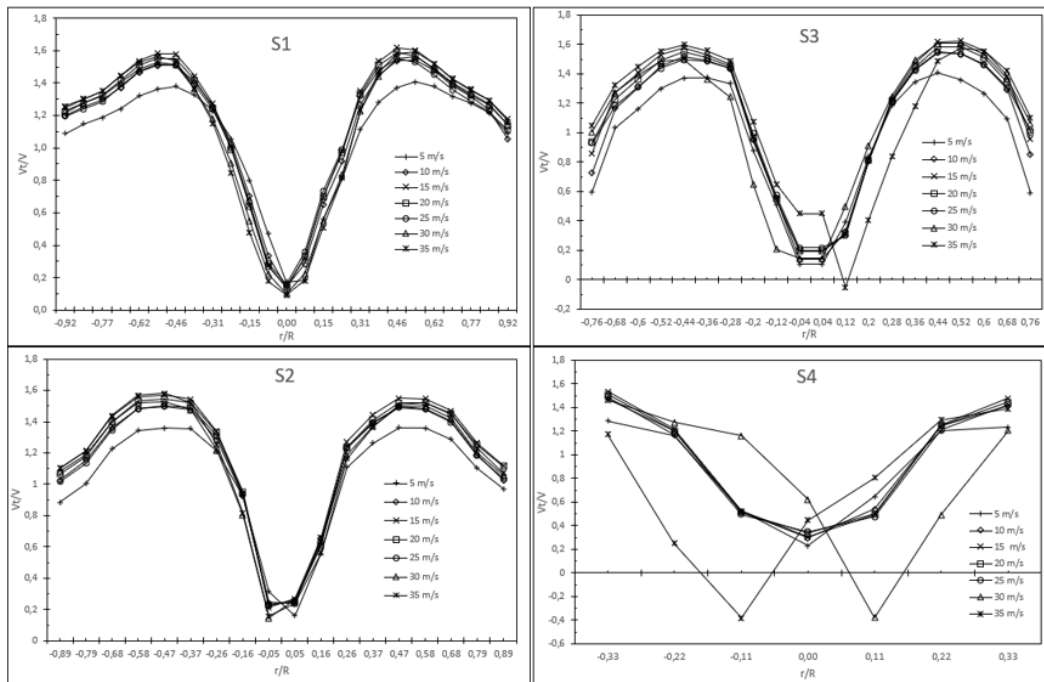

Figure 6. Tangential velocity profiles at different axial locations and inlet velocities.
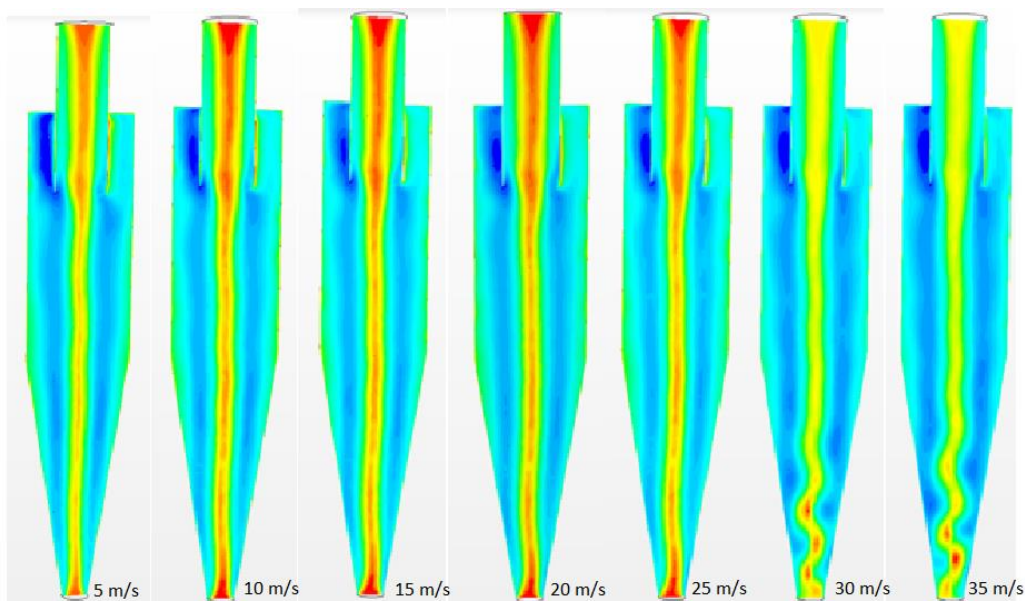
Figure 7. Tangential velocity contours at different inlet velocities.

3.3 Axial velocity

The axial force is vital to the separation efficiency; it affects the downstream discharge and its residence time. To be noted, higher residence time leads to more efficient separation. The axial force pushes the particles against the wall of the separator, which increases the centripetal accelerations. With the aid of gravitational force, high forces are exerted on the particles driving them to spin around along the walls of the separator. Fig. 8 shows the axial velocity profiles at different cross-sections inside the separator. The inlet velocity varies from 5 m/s to 35 m/s. At axial locations 1, 2 and 3, the mean velocity profiles are symmetric for all inlet velocities. However, at axial location 4, there is a pattern of irregularities. Also, it was observed that the shape of the mean axial velocity varies from W-shape at axial location 1, to U-shape and V-shape at axial locations 2 and 3, respectively. Furthermore, it is noted that there are some changes in the rotational characteristic of the flow when the velocity exceeds 30 m/s, as shown in Fig. 9. The inner vortex of the separator is no longer at the bottom part of the separator. Unlike the tangential velocity, the axial velocity is not symmetric with the axis of the separator [27].
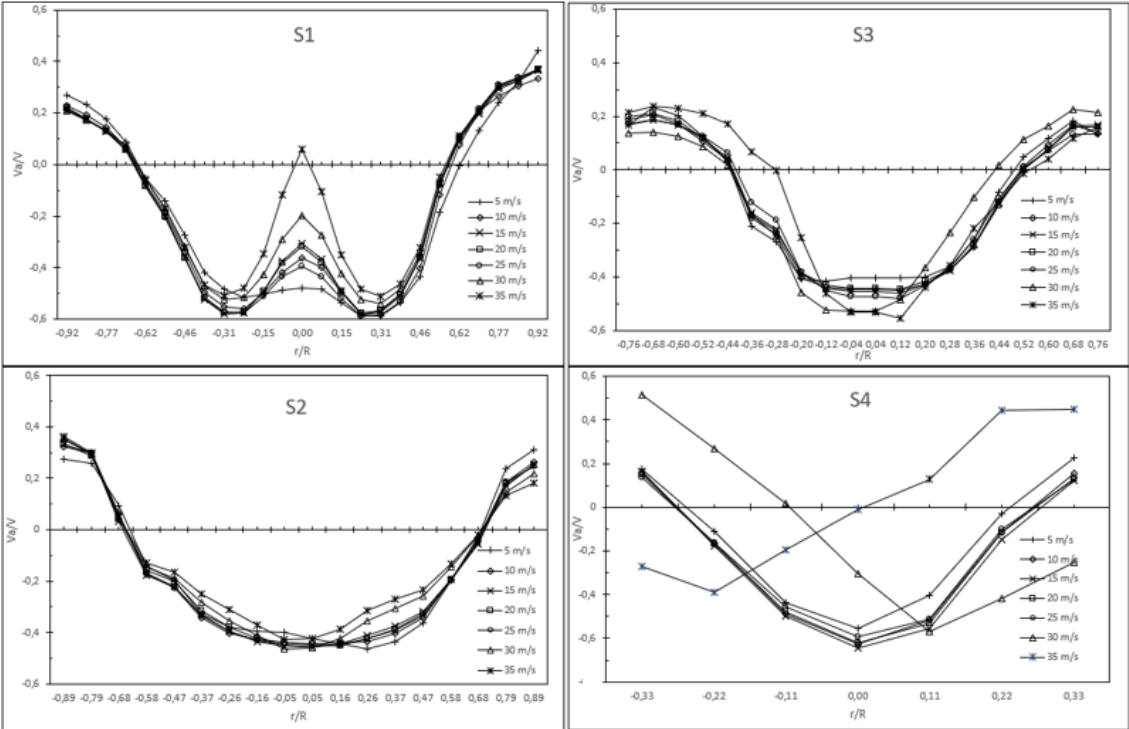
Figure 8. Axial velocity profiles for different cross sections at different inlet velocities.
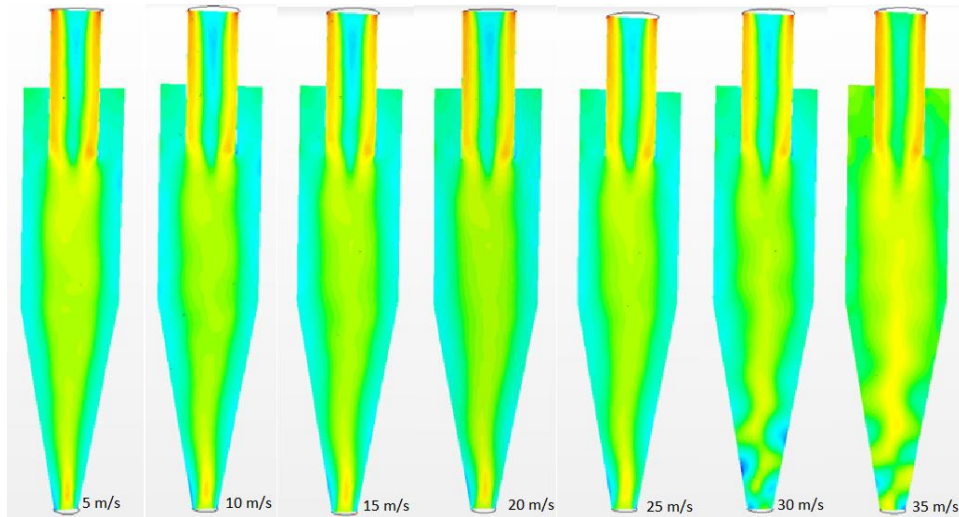
Figure 9. Axial velocity contours with different inlet velocities.

3.4 Separation efficiecny

One of the most significant parameters of the cyclone separators is its efficiency, which is greatly influenced by both the size of the particles and the inlet velocity. Fig. 10 represents the separation efficiency as a function of the diameter of the particles. Centripetal force influences larger particles by carrying them out toward the walls of the separator, which then fall downwards by gravity. Thus, as one would expect, the separation efficiency increases with increasing particle diameter. Particles with size higher than 3 μm, will lead to a separation efficiency close to 100%. The lighter particles will be captured by the inner vortex and then follow the flow to the top exit.

Fig. 11 shows the separation efficiency as a function of the inlet velocities. The computed results are in acceptable agreement with the experimental measurements with an average error of less than 6%. Also, the results indicate that separation efficiency is high for high inlet velocities because increasing inlet velocity leads to a higher centripetal acceleration acting on the particles.
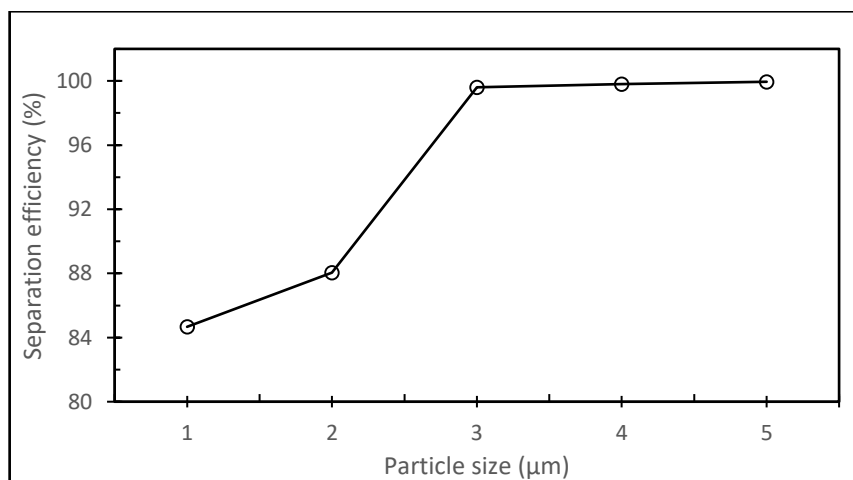

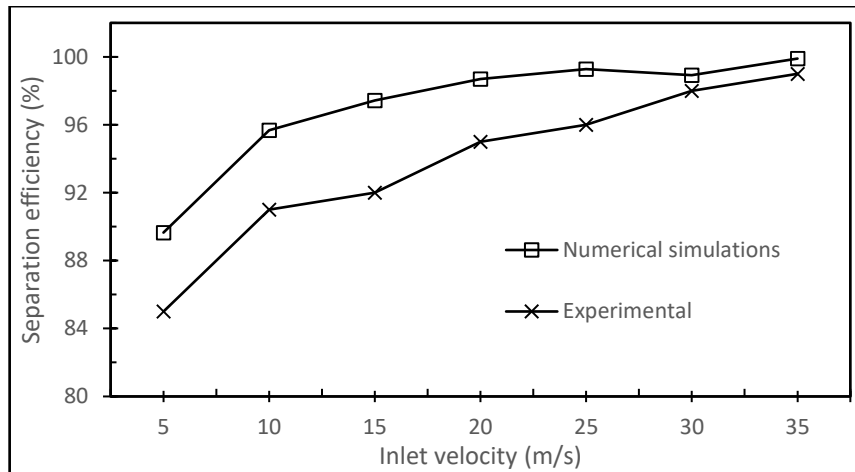Figure 10. Particle separation efficiency as a function of particle diameter.

Figure 11. Particle separation efficiency as a function of inlet velocity compared with calculated results and previous simulations.

Two different approaches were used in this study to determine the effectiveness of the separator; the Rosin-Rammler particle distribution (Eq. (15)), and a constant diameter for the particles entering the separator. Fig. 12 compares the separation efficiency of these two approaches as a function of inlet velocity. It shows that when using a constant particle diameter (5 μm), the separation efficiency is greater than using the Rosin-Rammler distribution. As previously presented, the separation efficiency increases with both inlet velocity and particle diameter, which explains why the constant diameter has a higher efficiency. However, the Rosin-Rammler is the most viable approach, since it provides a more realistic description of the particle size distribution in a physical separator.
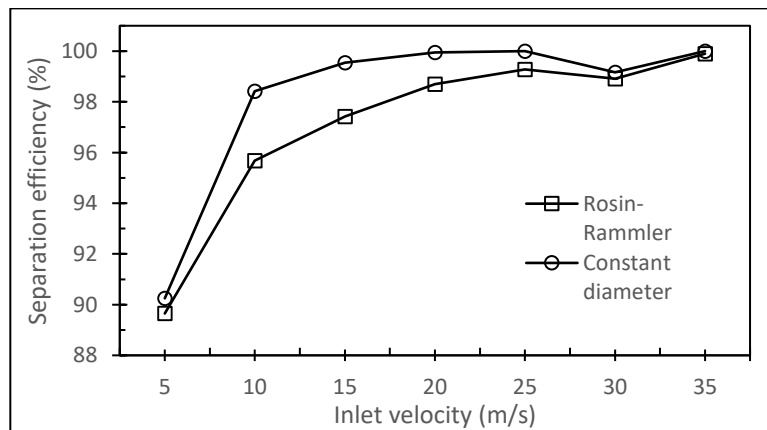

Figure 12. Comparison of separation efficiency as a function of inlet velocity, using Rosin-Rammler and constant particle diameter (5 μm).
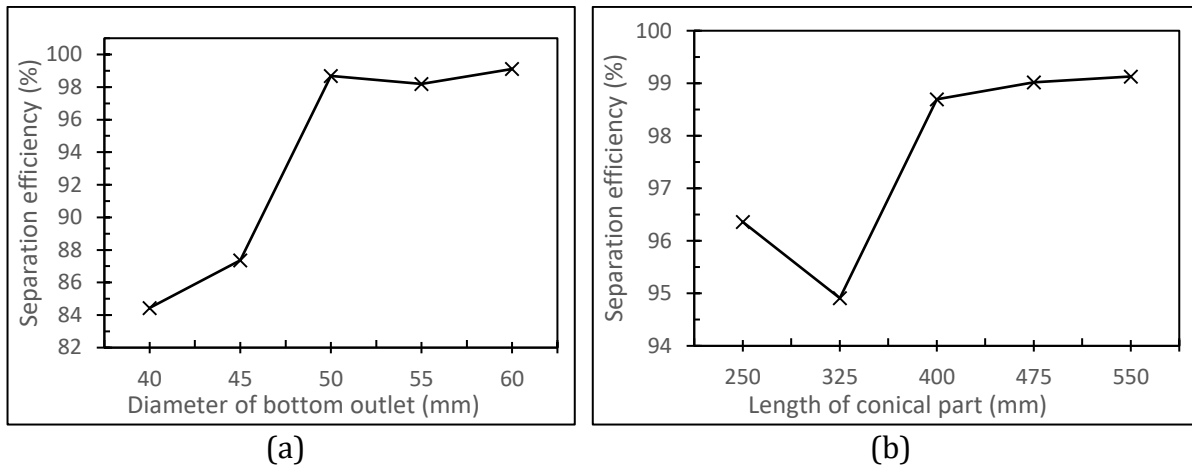
3.5 Geometric changes

(a)

(b)

Figure 13. Separation efficiency as a function of (a) diameter of the bottom outlet, and (b) length of the conical part.

There are several different ways to design a cyclone separator. By altering the geometric parameters, the results of the separation process sway. This is shown in Fig. 13 where two geometric parameters were altered to see the effects of these changes. In Fig. 13a the diameter of the bottom outlet is varying from 40-60 *mm* diameter, where 50 *mm* is the original diameter for the separator. It can be observed that the separation efficiency decreases when the outlet diameter decreases, while it is slightly increasing when the diameter increases. When reducing the diameter of the bottom outlet, the particles are easier caught in the vortex instead of escaping through the outlet.

Fig. 13b show how the efficiency is influenced by changing the length of the conical part of the separator, without changing the total length. The original length is 400 *mm*, and it varies from 250-550 *mm* in length. The represented results illustrate that the efficiency increases when the length of the conical part increases, and the opposite for when the length decreases. The conical part of the separator greatly influences the residence time of the particles, because it increases the centripetal force acting on the particles. This means that it will be tougher for the vortex to capture the particles and carry them up towards the top outlet. The comparison of the two geometric modifications depicts that the change in outlet diameter impact the results more than the length of the conical part.
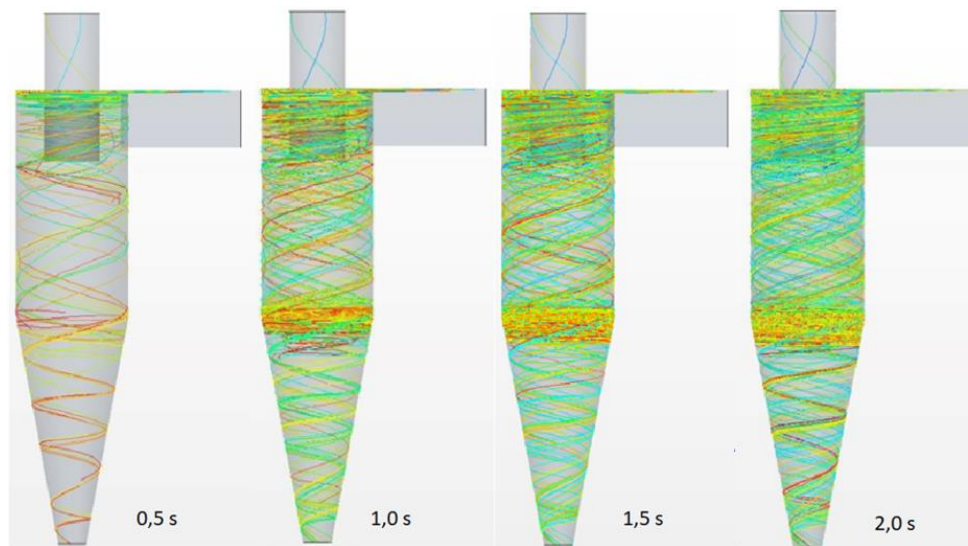
3.6 Particle flow pattern

Figure 14. Flow pattern of particles at different stages of the simulation.

Fig. 14 represents the flow pattern of the particles at four different stages of the simulation. For simplicity, only one of the particle injectors were used when tracking the particles. The different injectors will give different tracks, depending on their position on the inlet [12]. The injector in the profiles in Fig. 14 is in the upper right corner. For each of the stages, the red coloured tracks represent the particles with the highest residence time, while the teal colour represents the particles with the lowest residence time. At the first stage, the flow pattern shows that most of the particles are bundled together at the top of the separator, while a few particles descend towards the bottom outlet.

The second stage depicts how the pattern evolves from the first stage. The bundle of particles at the top increases, because the total amount of particles increases. In the second stage, there is a second collection of particles at the top of the conical body. When the flow pattern evolves into the next stage, it is evident that both collections of particles increases, and there are more particles exiting the separator through the bottom.

The final stage proves the same trend as previously described. Both the collections of particles increase, and more particles exit the separator. In this stage it is evident that a few of the particles have been caught by the vortex and forced up through the top outlet. The particle bundle at the top of the conical body is a good representation of how the particle separation process is executed. The large and heavy particles are forced downwards because of gravity. When the particles reach the conical part, the centripetal force acting on them increases to a level where gravity does not exert enough force to pull the particles further down, as observed in Wangs experiment [12]. This leads to a clustering of particles, as represented in Fig. 14. The simulations do not include interaction between the particles, so the number of particles exiting the separator would increase for a physical separator.

3.7 Discussion:

For this study, the RANS computational approach was used because of its simplicity. This approach gives an adequate representation of the results, but it's the least accurate method of the three listed in section 2. This approach has the lowest computational demand of the three, but the LES approach has become more common for engineering purposes. The LES approach gives a more accurate result but is more computational demanding. Since the number of iterations for the simulations was set to 20 000, the RANS model was the best option.

To study the flow of the particles inside the separator in an accurate matter, the timestep was set to 0,01, and 100 iterations is equal to one timestep. This made the simulations more computational demanding, but the results became more accurate. To study the flow patterns of the particles, the total time was set to 2 seconds, which led to high number of iterations. To be able to study how the flow patterns evolved over time, 20 000 iterations was required, even though the solution converged after about 6000 iterations. The results could have been obtained with a smaller timestep combined with less iterations, but the results would be less accurate.

The particles entering the separator was modelled using two different methods. The first used a constant diameter for the particles, while the second used the Rosin-Rammler equation to express the particle distribution. From the results, particles with a fixed diameter gave the best results, but this would be unlikely for a physical separator. For the simulations in this study the preferred method was the Rosin-Rammler distribution. Instead of having a set number of particles entering the separator, a specific volume flow of 0.003 m^3/s was set, which made the simulations more demanding. This made the particle flow pattern harder to study. To simplify the simulations, the number of particles entering the separator could have been given a constant number.

The simulations were set to use a one-way coupling scheme. This means that there is only interaction from the fluid phase on the particles, and the effects of particles on the fluid is neglected. The Lagrangian model also excludes particle-particle interaction inside the separator. In practice, the fluid phase would interact with the particles, and the particles would collide with each other. The collision between the particles would change the flow pattern of the particles.

4. Conclusion

This study represents a detailed numerical simulation of a two-phase cyclone separator using a multi-phase Eulerian-Lagrangian gas flow model. The computational results obtained are compared to the experimental results of Wang [12].

The computed pressure drop was in good agreement with experimental measurements at different inlet velocities. It has been noted that the computed pressure drops increases with an increase in the inlet velocities, which increases the separation efficiency, but makes the separation operation costly. The model was able to mimic the two distinctive symmetric vortices inside the separator. The tangential velocity was also computed and compared to the experimental measurements at different axial locations inside the separator. The axial force is vital to the separation efficiency; it affects the downstream discharge and the residence time and hence the axial velocity profiles for different cross sections at different inlet velocities. The separation efficiency was measured using two different approaches, and the comparison of these depicted that the constant diameter approach gave the best results, but this would be unlikely for a physical separator.

Even though there were some minor discrepancies between the measured and computed solution, the Eulerian-Lagrangian gas flow method has successfully mimicked the experimental measurement at different axial locations inside the separator, and the overall agreement was reasonably acceptable. The simulations were able to resemble the particle flow characteristics of a physical separator in an accetpable manner.

In further investigations, it would be smart to include the two-way coupling scheme. This would include the interaction from the dispersed phase on the fluid phase and give more accurate results. Increasing the physical time of the simulation would present a more improved depiction of the particle flow pattern.

References

[1]   L. Mølhave, S. K. Kjærgaard and J. Attermann, Sensory and other neurogenic effects of exposures to airborne office dust, *Atmospheric Environment,* vol. 34, pp. 4755-4766, 2000.

[2]   T. Schneider *et al.*, 'EUROPART'. Airborne particles in the indoor environment. A European interdisciplinary review of scientific evidence on associations between exposure to particles in buildings and health effects, *Indoor Air,* vol. 13, pp. 38-48, 2003.

[3]   D. Bradley, *The hydrocyclone*. 1965.

[4]   L. Svarovsky, *Solid-Liquid Separation : 6 - Hydrocyclones, 4th ed.*, Oxford: Butterworth-Heinemann, 2001, pp. 191-245.

[5]   J. M. Campbell, *Gas conditioning and processing : 2 - The equipment modules, 7th ed.*,Okla: Campbell Petroleum Series, 1992.

[6]   K. W. Chu *et al.*, Understand solids loading effects in a dense medium cyclone: Effect of particle size by a CFD-DEM method, *Powder Technology,* vol. 320, pp. 594-609, 2017.

[7]   H. Yoshida, Y. Hayase, K. Fukui and T. Yamamoto, Effect of conical length on separation performance of sub-micron particles by electrical hydro-cyclone, *Powder Technology,* vol. 219, pp. 29-36, 2012.

[8]   B. Guo, *Petroleum production engineering : a computer-assisted approach*. Amsterdam: Elsevier, 2007.

[9]   A. Bahadori, *Natural gas processing : technology and engineering design*, Massachusetts; Kidlington, Oxford: Elsevier, 2014.

[10]   A. H. Nissan and V. P. Bresan, Swirling flow in cylinders, *AIChE Journal,* vol. 7, pp. 543-547, 1961.

[11]   A. Hoekstra, Gas Flow Field and Collection Efficiency of Cyclone Separators, *Delft University of Technology*, 2000.

[12]   B. Wang, D. L. Xu, K. W. Chu and A. B. Yu, Numerical study of gas–solid flow in a cyclone separator, *Applied Mathematical Modelling,* vol. 30, pp. 1326-1342, 2006.

[13]   B. Andersson *et al.*, *Computational Fluid Dynamics for Engineers*. Cambridge, United Kingdom: Cambridge University Press, 2011.

[14]   A. Faghri and Y. Zhang, *Transport Phenomena in Multiphase Systems : 4 - generalized governing equations for multiphase systems: averaging formulations*, Boston: Academic Press, 2006, pp. 238-330.

[15]   S. Subramaniam, Lagrangian–Eulerian methods for multiphase flows, *Progress in Energy and Combustion Science,* vol. 39, 2012.

[16]   K. Hanjalić and B. Launder, *Modelling Turbulence in Engineering and the Environment: Second-Moment Routes to Closure*. Cambridge, United Kingdom: Cambridge University Press, 2011.

[17]   L. Schiller and A. Naumann, A drag coefficient correlation, *Z. Ver. Deutsch. Ing,* vol. 77, pp. 318-320, 1935.

[18]   Utikar *et al.*, *Hydrodynamic Simulation of Cyclone Separators*, 2010.

[19]   J. J. Derksen and H. E. A. V. d. Akker, Simulation of vortex core precession in a reverse-flow cyclone, *AIChE Journal,* vol. 46, pp. 1317-1331, 2000.

[20]   J. J. Derksen, Separation performance predictions of a Stairmand high-efficiency cyclone, *AIChE Journal,* vol. 49, pp. 1359-1371, 2003.

[21]   K. Elsayed and C. Lacor, The effect of cyclone vortex finder dimensions on the flow pattern and performance using LES, *Computers & Fluids,* vol. 71, pp. 224-239, 2013.

[22]   G. Alfonsi, Reynolds-averaged navier–stokes equations for turbulence modeling, *Applied Mechanics Reviews,* vol. 62, 2009.

[23]   P. Rosin, The Laws Governing the Fineness of Powdered Coal, *J. Inst. Fuel.,* vol. 7, pp. 29-36, 1933.

[24]   M. Peric and S. Ferguson, The advantage of polyhedral meshes, *Dynamics,* vol. 24, pp. 45, 2005.

[25]   L. Theodore, *Air pollution control equipment calculations : 9 - Cyclones*, N.J.: John Wiley & Sons, 2008, pp. 361-398.

[26]   S. V. Alekseenko, P. A. Kuibin, V. L. Okulov and S. I. Shtork, Helical vortices in swirl flow, *Journal of Fluid Mechanics,* vol. 382, pp. 195-243, 1999.

[27]   J. C. Cullivan, R. A. Williams, T. Dyakowski and C. R. Cross, New understanding of a hydrocyclone flow field and separation mechanism from computational fluid dynamics, *Minerals Engineering,* vol. 17, pp. 651-660, 2004.

List of figures

List of tables

Appendix 1

This appendix contains the detailed steps of creating the simulation in Star CCM+.

1. Creating the 3D-CAD model

The geometry of this model was created using Star CCM+ template 3D-CAD models. For a geometry as simple as this Star CCM+ can be used for drawing. However, the 3D-drawing for more complex geometries would be much harder with Star CCM+ compared to other geometrics modelling software's such as Creo, inventor, Ansys or Autodesk.

The geometry is in three parts. The separator body, the upper outlet and the inlet. The separator body was cut in half and then revolved 360 degrees around the z-axes. The upper outlet was extruded from the middle of the separator body upwards. The inlet was extruded from the XY plane. The inlet and outlet faces were renamed and specified to its designated part. Rename the 3D-CAD model to cyclone.
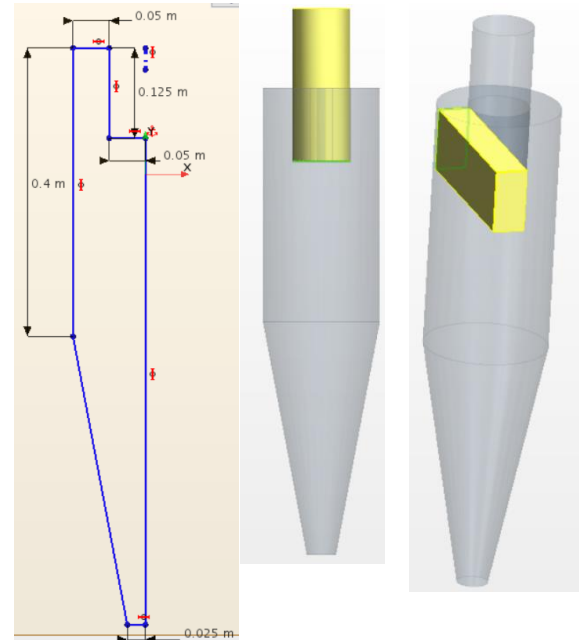

Figure 15. Skecth of separator

2. Creating a geometry part

To use the 3D-CAD model in a simulation, create a geometry part:

1. Right-click the **Geometry** > **3D-CAD Models** > **Cyclone** node and select **New Geometry Part**.

2. In the *Parts Creation Options* dialog, click **OK** to close the dialog. Leave the default settings as it is.

3. Expand the **Parts** > **Fluid** > **Surfaces** node.

The inlet and outlet faces that is specified in the previous section are defined as separate surfaces.

3. Assigning a part to a region

To define the computational domain, the cyclone separator parts were assigned to a region. Under the **Geometry > Parts > Fluid**, **Assign Parts to Region** was selected. Choose the following: create a region for each part and a boundary for each part surface. A geometry scene is created to verify each part is correct.

4. Selecting physics models

Select the physics models

1. Create the physics continuum
2. For the physics continuum, **Continua > Physics 1**, select the following models in order:

Group box	Enabled Models
Space	Three dimensional
Time	Implicit unsteady
Material	Gas
Flow	Segregated flow
Equation of state	Constant density
Viscous regime	Turbulent
Reynolds-averaged turbulence	Reynolds stress turbulence
Reynolds stress turbulence models	Linear Pressure Strain Two-layer
Optional models	Gravity Lagrangian multiphase Segregated fluid isothermal

Table 3. Physics continum.

There are three things that must be changed under physics models:

1.The density of air, under **Gas** node

2.Lagrangian multiphase will be mentioned below

3.The temperature under **Segregated Fluid Isothermal** node

5. Lagrangian multiphase

Create the Lagrangian phase and select the appropriate phase models. These models represent the characteristics of the Lagrangian phase. To create the Lagrangian phase and select the phase models. In the **Physics 1** continuum, right-click the **Models** > **Lagrangian Multiphase** > **Lagrangian Phases** node and create a new phase. For the **Phase 1**, select the following models:

Group box	Model
Particle type	Material Particles Pressure Gradient Force (Selected automatically) Spherical Particles (Selected automatically)
Material	Solid
Equation of state	Constant density
Track sampling	Track file
Optional particle forces	Drag force

	Virtual mass
Optional models	Turbulent dispersion

Table 4. Lagrangian multiphase models

When the Lagrangian phase is made, the density of the solid must be changed. Right-click the **Solid** node then **Al > Material properties > Density > Constant > Value** and change the value to the right density.

6. Generating the volume mesh

Use a polyhedral mesh to analyse the flow patterns in the cyclone separator.

1. Right-click the **Geometry** > **Operations** node and
   select **New** > **Mesh** > **Automated Mesh**.
2. In the *Create Automated Mesh Operation* dialog:

   a. Select **Fluid** from the *Parts* list.

   b. Select the following meshers, in order:

Group	Mesher
Surface meshers	Surface remesher
Core volume meshers	Polyhedral mesher
Optional boundary layer meshers	Prism layer mesher

Table 5. Mesh selctions

   c. Click **OK**.

   An automated mesh operation is added to the **Operations** node.

3. Select the **Automated Mesh** > **Default Controls** > **Base Size** node and set **Value** to 0.0075 *m*. Select the **Number of prism layers** and set the value to 4.

   Right click the **Automated mesh > Execute** and the mesh will be set. Or

   Click **(Generate Volume Mesh).**

7. Specifying boundary conditions

Specify conditions at the inlet and outlet boundaries:

1. Edit the **Regions** > **Fluid** > **Boundaries** node.

2. Set the following properties:

Node	Property	Setting
Inlet	Type	Velocity inlet
└ **Physics Conditions** > Turbulence Specification	Method	Intensity + viscosity ratio

└ **Physics Values** > Velocity Magnitude	Value	20 *m/s*
└ **Physics Values** > Turbulence intensity	Value	0.01
└ **Physics Values** > Turbulence viscosity ratio	Value	10.0
Outlet 1	Type	Pressure outlet
Outlet 2	Type	Pressure outlet

Table 6. Selections of boundary conditions.

8. Setting up the injector

Set up an injector to introduce the particles of the dispersed Lagrangian phase into the solution domain. The injector defines the initial state of the particles.

To set up the injector:

First a derived part must be made. Right-click on the **Derived Part** node, then **New part > Probe > Presentation Grid**. This grid must be set at the inlet, a few cm in. To get 128 injectors where the particles will spawn, the grid is 16 in x-resolution and 8 in y-resolution. Meaning 8 particle injectors in width and 16 particle injectors in length.
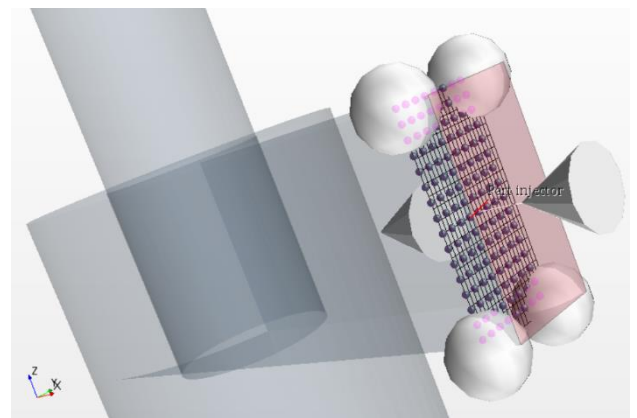
Now the injector settings must be set:

Figure 16. Presentation grid for injectors

1. Right-click the **Injector** node and select new
2. Select the **Injectors > Injector 1** node and right-click then edit.
3. Set **Lagrangian Phase** to **Phase 1**.
4. **Type** to **Part injector**
5. Set **Inputs** to **Derived parts > Presentation grid**
6. Click **Close**
7. Open the **Injectors** > **Injector 1** node.
8. Edit the following in the **Condition** node and set the appropriate properties:

Node	Property	Setting
Flowrate distribution	Method	Per injector
Flow rate specification	Method	Volume flow rate
Particle size specification	Method	Particle size
Velocity specifications	Method	Components
	Reference frame	Absolute

Table 7. Injector settings.

9. Edit the following in **Values** node:

Node	Property	Setting
Particle Diameter	Method Min (value) Max (value) Reference (value) Exponent (value)	Rosin-Rammler 1.0E-6 m 1.0E-4 m 2.99E-5 m 0.806
Velocity	Method Value Coordinate system	Constant [-20.0,0,0] Laboratory
Volume flow rate	Method Value	Constant 0.003 m^3/s

Table 8. Injector values

Note: The velocity must be in the direction of the inlet towards the cyclone. In this case negative X direction. The volume flow rate of the solid is 3% of the volume air flow rate. The volume flow of air was calculated by taking the area of the inlet (m^2) multiplied with the velocity (m/s), then multiply again with 0.03 (3%) to get the volume flow rate of the solid.

9. Setting up particle tracks

From the start of the simulation the particles must be tracked. They are tracked before every simulation and needs to be changed if different simulations are performed. Under the **Solver > Lagrangian multiphase > Track file** there are two settings that needs to be edited:

Export Directory	The directory to which the track file is exported. The default value is ". " and means the same directory as the .sim file.
Base Name	The name of the track file, without the .trk extension. The default is empty, in which case the track file has the same name as the .sim file.

Table 9. Trackfile settings.

To see the efficiency of the separator many different methods can be used. In this simulation it was done by making two plots at each outlet. In these plots particles that exited the different outlets could be counted. To see the number right-click the scene and tabulate, here every single particle will come up and give its location.
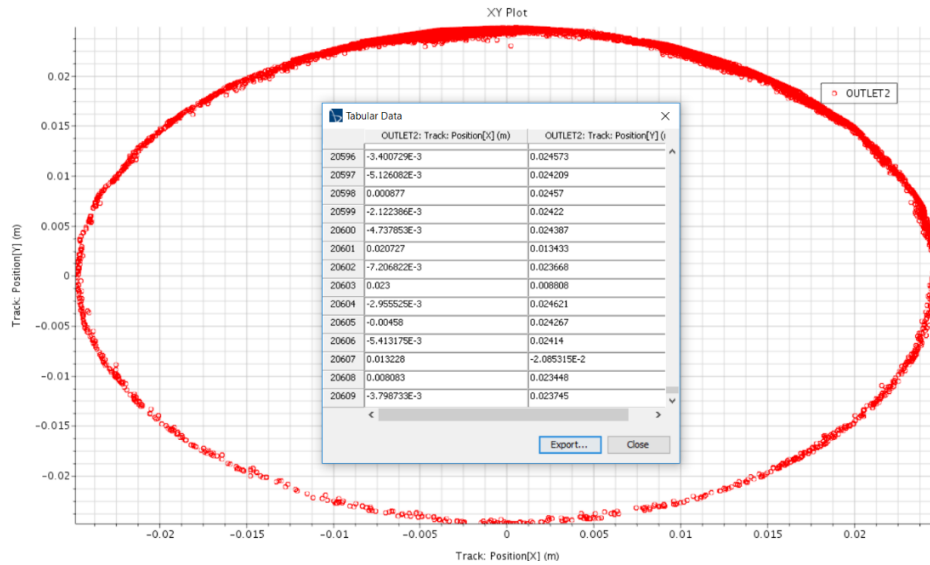
Figure 17. Plot of particle distribution.

To make this plot two things must be done:

1. Right-click the node **Derived part** and make a new section plane. The plane must be placed at the outlet very close to the edge, but make sure it's on the inside of the separator. This must be made for each outlet. Name it to make it easier later to see where the different planes are positioned.

2. Right-click the node **Plots** > **New plot > XY plot**. Right-click the newly made XY plot and edit it.

Node	Values
XY plot	-
└ Title	Upper/lower outlet
└ Parts	The section plane which is made above. Must fit the right outlet
X Type	-
└ Type	Scalar
└ **Scalar function**	-
└ Field function	Track: Position [X]
└ unit	*m*
Y types	**-**
└ Type	Scalar
└ Units	*m*
└ Smooth values	✓
└ **Scalar function**	**-**
└ Field function	Track: Position [Y]
└ Units	*m*

Table 10. Plot settings.

The simulation is now set up for particle tracks. After the simulation is done the newly made track file must be selected for the simulation. Under **Tools > Particle tracks** right click, then **Track file.** Select the track file and it will be assigned to the simulation. This can be verified with the new **Particle tracks** node appearing. To make the particles appear on the plot, edit the section planes for the top and bottom outlet made earlier. Edit the **Parts** section and select **Particle tracks.**

10. Stopping criteria

Stopping criteria specifies how long the solution runs for and under what conditions it stops iterating or marching in time. There is three ways to automatically stop the simulation. **Maximum inner iterations, Maximum physical time** and **Maximum steps.** For this simulation, 2 seconds physical time is enough. The simulation would take too long to calculate if the physical time increases. Increasing the stopping criteria for **inner iteration** and **steps** to make sure they won't stop the simulation**.** Then set a constraint on 2 seconds on **physical time,** the simulation doesn't need to be supervised during simulation and will stop at the set time.

11. Timestep

Simulations was performed in the implicit unsteady fashion with a time step 0.01 second. The standard timestep is set as 0.001. With this timestep the simulation would increase its accuracy but will take 10x longer to simulate. To change this value, go to **Solvers > Implicit unsteady** edit the time-step to 0.01 second from 0.001. This new timestep will be accurate enough and simulate in a reasonable time.

12. Running the simulation

The preparation of the simulation is now complete, and the simulation can be run.

1. Click on the green **Initialize solution** flag
2. Click (**Run**) in the *Solution* toolbar.
3. When the simulation has finished iterating, save it.

13. Creating a line probe

To check the tangential and axial velocities in a XY-plane, line probes is used. Click **Derived parts > New part > Probe > Line...** and make the line probe go across the separator. The **Resolution** changes the number of points across the line probe. The name of the line probe can be changed if many line probes are in use.
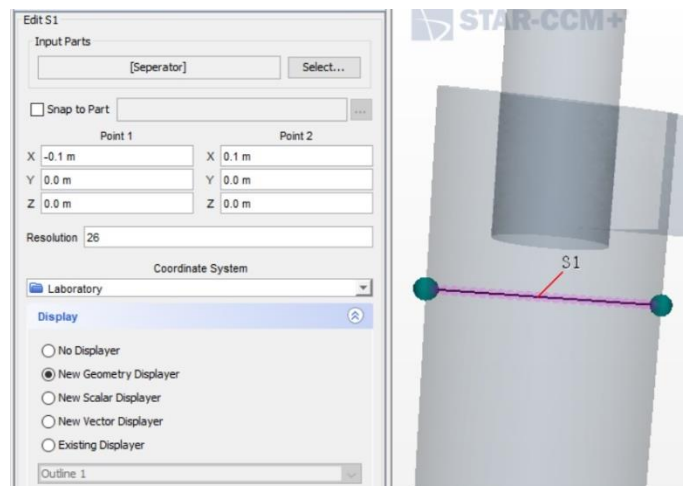

Figure 18. Line probe setup.

Create an XY plot. Right-click the **Plots** node and select **New Plot** > **XY Plot**. Expand the **XY Plot 1** node and set the properties.

XY plot	-
└ Title	XY plot
└ Parts	S1 *(line probe made)*
X Type	-
└ Type	Direction
└ **Vector quantity**	-
└ Value	[1.0, 0.0, 0.0] *m*
Y types	**-**
└ Type	Scalar
└ Units	*m*
└ Smooth values	✓
└ **Scalar function**	**-**
└ Field function	Tangential velocity
└ Units	*m/s*

Table 11. Plot settings.

Here is 4 different line probes shown in one plot. Add the different probes to **Part** node in **XY-plot**. To change the visualisation of the plot the axes can be modified, edit the **Axes** node. The lines can also be changed, under **Y-types > S1 > Line style**.
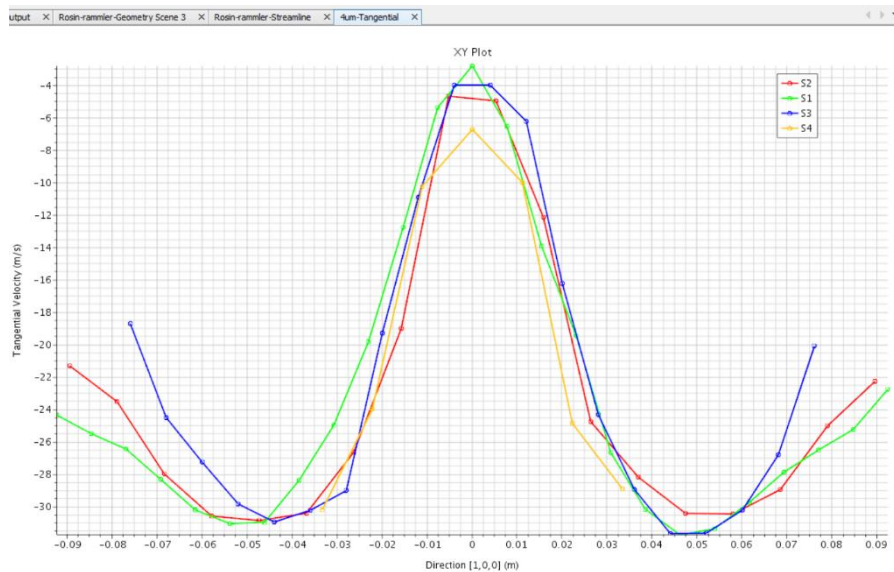
Figure 19. Plot of line probes

14. Preparing a scalar scene

To check the results, a scalar scene can be made. First create a section plane in the **Derived part** node. This plane will go straight through the separator as shown on the picture. Then a new scalar scene must be made in the **Scene** node. Go to the top left, beside **Simulation** there will be a **Scene/plot** button. Click this after opening the scalar scene that's been made. Here the scene settings will be defined. Go to **Scalar 1 > Parts** and edit. Select the **Derived parts** and select the section plane made for the scalar scene. To visualize the results, use **Scalar field** > **Function** and select function too i.e.: Axial velocity, tangential velocity, static pressure etc.
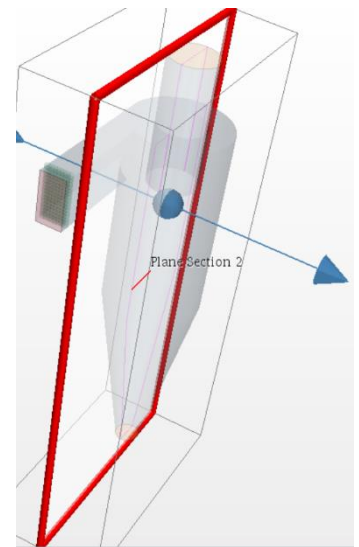
15. Creating a streamline scene

Create a scene to display the streamlines inside the cyclone separator.

Figure 20. Section plane.

1. Create a Geometry Scene.

2. Rename the **Geometry Scene 2** node to Streamlines.

Use the *Create Streamline* panel to specify the properties of the streamlines. In this case, the streamlines will start from the cyclone inlet.

3. Create a Streamline derived part with the following properties:

Property	Setting
Input parts	Regions > fluid

Seed parts	Regions > separator > boundaries > inlet
Optional boundary layer meshers	Prism layer mesher
Part U-resolution	2
Part V-resolution	8

Table 12. Streamline settings.

Define the scene settings:

4. Click **Scene/plot**.

5. Edit the **Streamlines** > **Displayers** node and set the following properties:

Node	Property	Setting
Displayers	-	-
└**Geometry 1**	Opacity	0.3
└Streamline stream 1	Mode	Ribbons
└Scalar Field	Function	Velocity > Lab reference frame > laboratory > k

Table 13. Streamline display settings.

To extend the streamlines through the fluid domain up to the outlet, increase the maximum propagation property. This defines how far the streamlines are propagated through the fluid domain from the starting points. A higher value causes the streamlines to extend further.

6. Click the **Simulation** button.

7. Select the **Derived Parts** > **Streamline** > **2nd Order Integrator** node and set **Maximum Propagation** to 15.

8. Streamlines can also be made for particle tracks. Under **Scene/plot > Displayers > Streamlines > Parts** add the particle tracks to the part instead of the derived part.

16. Pressure drop report

Pressure drop can be made as a report in Star CCM+, which means it calculate itself.
Click **Reports > New report > [Element count...Surface integral] > Pressure drop**.
A new report has been made, edit the **Pressure drop 1**.

Nodes	Values
Units	*Pa*
High Pressure	[Separator: inlet]
Low Pressure	[Separator: Outlet top, Separator: Outlet down]

Table 14. Pressure drop report.

The pressure drop report is set. After the simulation is done, report can be right clicked and **Run report** can be selected. This will give the value of the pressure drop in the **Output** of the simulation.